

High-pressure transport properties of CeRu₂Ge₂

H. Wilhelm¹, D. Jaccard², V. Zlatić³, R. Monnier⁴, B. Delley⁵, and B. Coqblin⁶

¹*Max-Planck-Institut für Chemische Physik fester Stoffe, Nöthnitzer Str. 40, 01187 Dresden, Germany*

²*Département de Physique de la Matière Condensée, Université de Genève,
Quai Ernest-Ansermet 24, 1211 Genève 4, Switzerland*

³*Institute of Physics, Bijenička cesta 46, P. O. Box 304, 10001 Zagreb, Croatia*

⁴*ETH Hönggerberg, Laboratorium für Festkörperphysik, 8093 Zürich, Switzerland*

⁵*Paul Scherrer Institut, WHGA/123, 5232 Villigen PSI, Switzerland and*

⁶*Laboratoire de Physique des Solides, Université Paris-Sud, Bât. 510, 91404 Orsay, France*

The pressure-induced changes in the temperature-dependent thermopower $S(T)$ and electrical resistivity $\rho(T)$ of CeRu₂Ge₂ are described within the single-site Anderson model. The Ce-ions are treated as impurities and the coherent scattering on different Ce-sites is neglected. Changing the hybridisation Γ between the 4f-states and the conduction band accounts for the pressure effect. The transport coefficients are calculated in the non-crossing approximation above the phase boundary line. The theoretical $S(T)$ and $\rho(T)$ curves show many features of the experimental data. The seemingly complicated temperature dependence of $S(T)$ and $\rho(T)$, and their evolution as a function of pressure, is related to the crossovers between various fixed points of the model.

PACS numbers: 75.30.Mb, 72.15.Jf, 62.50.+p, 72.15.Qm, 71.27.+a

I. INTRODUCTION

The thermoelectric power (S) of Ce-based heavy fermion (HF) or unstable valence compounds and alloys exhibits a seemingly complicated temperature dependence, $S(T)$. Depending on the hybridisation (Γ) between the 4f and the conduction electrons, the systems can attain ground states varying from magnetically ordered to mixed valent (MV), like CeCu₂Ge₂ [1] and CeNi₂Si₂ [2], respectively. Between these two extreme cases magnetic Kondo systems, e.g. CeAl₂ [3], and HF compounds like CeCu₂Si₂ [4], CeRu₂Si₂ [5], and CeCu₆ [6] are situated. A systematic development of pronounced features in $S(T)$ becomes apparent if the compounds are arranged according to increasing Γ -values, i.e. upon approaching the MV regime.

One possibility to increase Γ in Ce-compounds is to apply pressure (p). Depending on the compounds' ground-state properties (i.e. the value of Γ) at ambient pressure, some of the anomalies at low and high temperature evolve and their behaviour under pressure can be studied. Examples for the influence of pressure on $S(T)$ of a magnetically ordered compound are CeCu₂Ge₂ and CePd₂Si₂ [1, 7, 8]. In the case of HF systems, pressure effects on $S(T)$ of CeAl₃ and CeCu₂Si₂ [4, 9] were explored intensively. The transport properties of the magnetically ordered CeRu₂Ge₂ clearly revealed the pressure-induced development of two well resolved maxima in $S(T)$ over a considerably large pressure range [10]. The development of a pronounced positive maximum close to room temperature is related to the splitting of the 4f states due to the crystalline electric field (CEF) [11]. The non-monotonic $S(T)$ below about 10 K is very likely caused by the occurrence of magnetic order and the opening of a gap in the magnetic excitation spectrum. Upon approaching the magnetic/non-magnetic phase boundary at a critical pressure $p_c = 7.8$ GPa, a low-temperature

maximum evolves above 10 K. It is very likely related to the Kondo effect and gives a measure of the Kondo temperature, T_K . Well above this pressure only the high-temperature maximum remains and the $S(T)$ -curves lose their complexity.

The anomalous $S(T)$ -data of Ce- and Yb-based compounds were subject of many theoretical investigations and are still discussed controversially (see Ref. [12] and references therein). In the present article we present a qualitative description of the pressure-induced changes in $\rho(T)$ and $S(T)$ of CeRu₂Ge₂ within the single-site Anderson model. The spectral function of the 4f-electron was obtained within the non-crossing approximation (NCA). The results above the characteristic energy scale T_0 can be used reliably, whereas for $T < T_0$ the limitations of the method should be kept in mind. An accurate solution of the single-impurity model at low temperature is not useful, because we are dealing with a stoichiometric compound, which is magnetically ordered at low pressure. A single-site model cannot describe ordered compounds below the coherence temperature anyway. Despite these limitations, the Anderson model yields a qualitative description of the experimental data of CeRu₂Ge₂ above the ordering temperature.

II. EXPERIMENTAL RESULTS

A clamped Bridgman anvil cell with synthetic diamonds was used to pressurise the sample up to 16 GPa. The four-point $\rho(T)$ and the $S(T)$ measurements were carried out on *one* sample in the temperature range $1.2 \text{ K} < T < 300 \text{ K}$. It is important to note, that $\rho(T)$ as well as $S(T)$ were measured perpendicular to the tetragonal c -axis. A general description of the experimental high-pressure set-up for $S(T)$ measurements can be found in Ref. [13]. The experimental results of interest

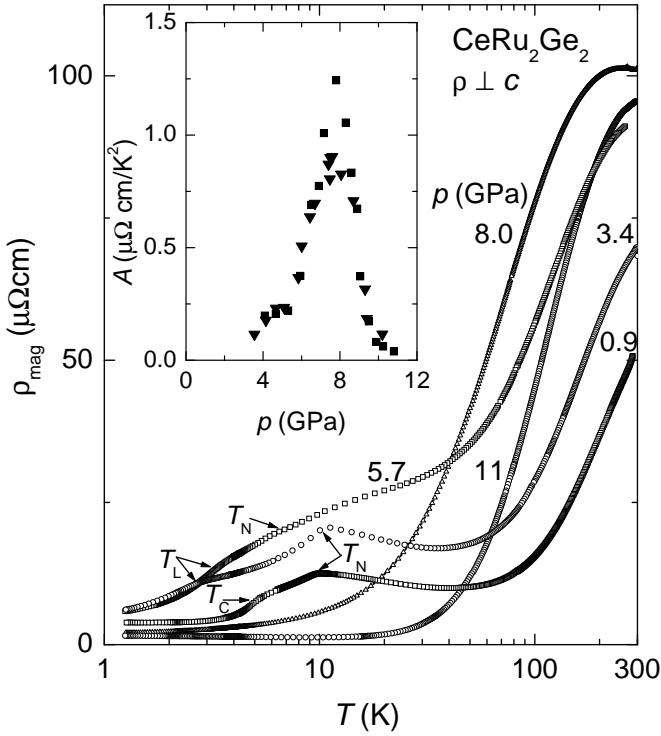


FIG. 1: Magnetic contribution $\rho_{mag}(T)$ to the electrical resistivity of CeRu_2Ge_2 at different pressures. Two different antiferromagnetic phases occur below T_N and T_L , and a ferromagnetic ground state is present below T_C and low pressure. No traces of magnetic order are observed for $p > 7$ GPa above 1.2 K. Inset: Pressure dependence of the A -coefficient obtained from a fit to $\rho(T) = \rho_0 + AT^2$ for $T < 0.5$ K to the data of Ref. [16].

in the present context are summarised in the following. A thorough presentation of the experimental findings can be found in Ref. [10].

The magnetic part $\rho_{mag}(T)$ of the total electrical resistivity, $\rho(T)$, is shown in Fig. 1. It was obtained by subtracting an appropriate phonon contribution [10]. In the region of interest here ($T > 10$ K), a maximum in $\rho_{mag}(T)$ develops near room temperature for intermediate pressures. Its origin is attributed to the Kondo exchange interaction between the conduction electrons and the crystal-field split ground state of the Ce^{3+} -ions.

This interpretation is supported by the evolution of a high-temperature maximum in $S(T)$ as can be seen in Fig. 2. Its position, T_S , corresponds to a fraction of the crystal-field splitting (the first excited doublet is at $\Delta = 500$ K [14, 15]) and its amplitude increases linearly with pressure up to a value of $55 \mu\text{V/K}$ at about 10 GPa. As in $\rho(T)$ the features in $S(T)$ below about 10 K and $p \leq 3.4$ GPa reflect presumably the appearance of long-range magnetic order [10]. At 5.7 GPa, however, a pronounced maximum at $T_K \approx 12$ K is present. Its position is very sensitive to pressure and a trace of it can be anticipated at about 40 K (see 8.0 GPa data shown in the inset to

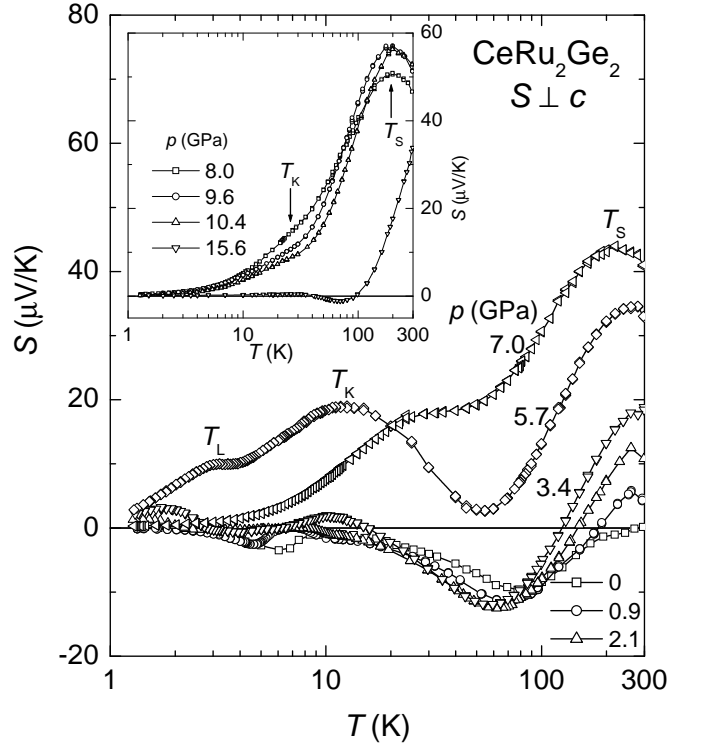


FIG. 2: Temperature dependence of the thermoelectric power $S(T)$ of CeRu_2Ge_2 for various pressures. The features present in the low temperature part of $S(T)$ for $p \leq 5.7$ GPa are due to the magnetic order (e.g. T_L). T_K and T_S label the centre of broad, pressure-induced maxima, related to the Kondo effect and the crystalline electric field, respectively. The inset shows $S(T)$ data of CeRu_2Ge_2 in the non-magnetic phase.

Fig. 2).

Based on these results as well as earlier transport [16, 17] and calorimetric measurements [18] a (T, p) phase diagram of CeRu_2Ge_2 can be drawn (Fig. 3). In the present context, the main observation is that the long-range magnetic order is suppressed at a critical pressure $p_c \approx 7.8$ GPa and that a HF like behaviour equivalent to that in CeRu_2Si_2 at ambient pressure sets in for $p > p_c$. The almost identical $S(T)$ curves of CeRu_2Si_2 at ambient pressure and CeRu_2Ge_2 at high pressure strongly suggest that the unit-cell volume is the crucial parameter as far as the size of the Kondo exchange interaction is concerned, and suggests that the position of the peak in $S(T)$ at low temperature is a measure for the Kondo temperature T_K [10]. Additional support for this assignment is provided by the pressure dependence of the $A(p)$ -coefficient (inset to Fig. 1) of the quadratic-in temperature $\rho(T)$ behaviour fitted to the data below 0.5 K reported in Ref. [16]. In the non-magnetic regime the assumption $T_K \propto 1/\sqrt{A}$ holds and the calculated $T_K(p)$ data are shown in Fig. 3 [10]. They were normalised in such a way that at $p = 7.8 + 0.6$ GPa the value of $T_K = 24$ K of CeRu_2Si_2 at ambient pressure was obtained [19]. The small pressure offset corresponds to the fact that long-range magnetic order

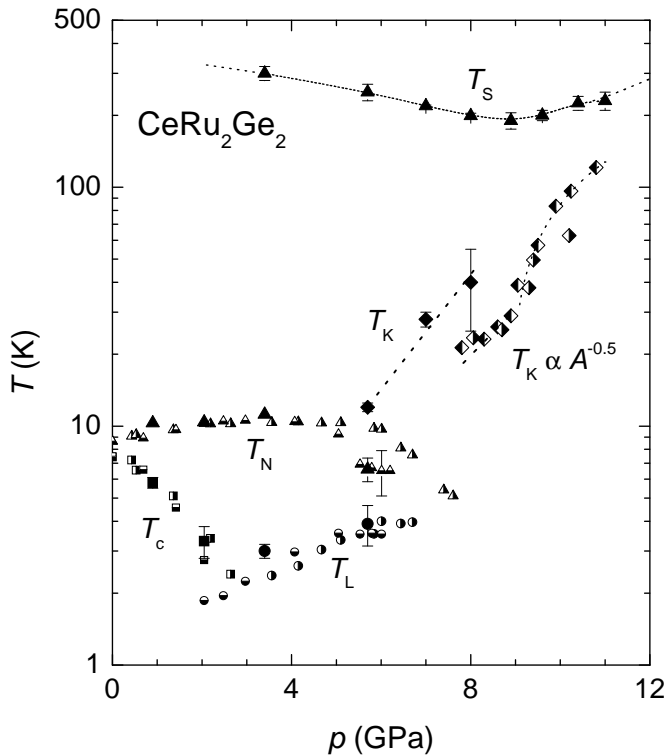


FIG. 3: Detailed (T, p) phase diagram of CeRu_2Ge_2 as obtained from electrical resistivity [16, 17], calorimetric [18], and the combined $\rho(T)$ and $S(T)$ (bold symbols) measurements [10]. The long-range magnetic order (T_N and T_L : antiferromagnetic, T_C : ferromagnetic) is suppressed at $p_c \approx 7.8$ GPa. T_S and T_K represent the centre of peaks in $S(T)$.

in $\text{CeRu}_2(\text{Si}_{1-x}\text{Ge}_x)_2$ vanishes at a critical concentration $x_c \approx 0.06$ [10, 20].

III. THEORETICAL MODEL

The theoretical description is based on an effective impurity model. It is assumed that the scattering of conduction electrons on a given Ce-ion depends on other Ce-ions only through the modification of the conduction band. Fluctuation between $4f^0$ and $4f^1$ configurations by exchanging electrons with the conduction band are allowed. The energy difference between the two configurations is $|E_f|$ and the hopping is characterised by the matrix element V . The $4f^1$ configuration is represented by the CEF states which are split by an energy $\Delta \ll |E_f|$. The local symmetry is taken into account by specifying the degeneracy of the CEF levels. The $4f^2$ configuration is excluded, i.e., an infinite strong repulsion between $4f$ -electrons is assumed.

A. Model hamiltonian

Taking the impurity concentration equal to one, and imposing that the average number of conduction electrons and $4f$ -electrons is conserved (self-consistency condition) [12], the Hamiltonian for the effective single-ion Anderson model is given by

$$H_A = H_{band} + H_{imp} + H_{mix}, \quad (1)$$

where H_{band} describes the conduction states, H_{imp} represents CEF states at E_f and $E_f^* = E_f + \Delta$, and H_{mix} gives the transfer of electrons between $4f$ and conduction states. All energies are measured with respect to the chemical potential μ . The properties of the model depend in an essential way on the CEF splitting Δ and the coupling constant $g = \Gamma/(\pi|E_f|)$, where $\Gamma = \pi V^2/W$ measures the coupling strength between the $4f$ -electrons and a semi-elliptical conduction band (centred at $E_0 > 0$) of half-width W . In the limit $\Gamma \ll 1$ and $\Gamma < \Delta$, the model represents the $4f^1$ configuration of the Ce ion at ambient pressure and high temperature. An increase of pressure stabilises the $4f^0$ configuration of the Ce-ion and enhances the configurational mixing. Therefore, the influence of pressure is accounted for by an increase of the hybridisation from $\Gamma < \Delta$ to $\Gamma > \Delta$. In a Kondo-lattice compound the hybridisation can give rise to charge fluctuations and in order to obtain charge neutrality, μ was adjusted at each temperature and hybridisation. Furthermore, it is assumed that pressure does not change Δ and W but shifts the bare f -level and the centre of the conduction band by the same amount. Thus, for a given Ce-compound, $n_c + n_f$ and $|E_0 - E_f|$ remain constant at all temperatures and pressures [21].

In order to describe the influence of pressure on $S(T)$ and $\rho(T)$ of CeRu_2Ge_2 , which is paramagnetic at high temperature and ambient pressure, it is sufficient to consider the case $g \ll 1$. The behaviour of the Anderson model in that limit is controlled by several well defined fixed points [22]. In the case of $\Gamma < \Delta$, the impurity appears to be magnetic and the low-temperature behaviour is characterised by the FL fixed point, which describes a singlet formed by the $4f$ -moment and the conduction electrons. An increase of temperature gives rise to a transition to the local moment (LM) fixed point, which characterises a CEF split $4f$ -state weakly coupled to the conduction band. This transition takes place around the Kondo temperature, T_0 , determined by g , Δ , and the degeneracy of the CEF states [23, 24]. The definition of T_0 in the NCA is given in the next section. The remarkable feature of the Anderson model is that the physics at the FL and the LM fixed points is governed by the same characteristic energy scale T_0 . A further transition to a fixed point related to the scattering of conduction electrons on an effective six-fold degenerate $4f$ -multiplet occurs at temperatures above Δ . In the case of $\Gamma \gg \Delta$, the impurity is in the non-magnetic MV regime.

The electrical resistivity and the thermopower of the single-impurity Anderson model are obtained from the usual expressions [25],

$$\rho_{mag} = \frac{1}{e^2 L_0}, \quad (2)$$

$$S = -\frac{k_B}{|e|T} \frac{L_1}{L_0}, \quad (3)$$

with k_B the Boltzmann constant and e the electronic charge. The transport coefficients L_0 and L_1 are given by the static limits of the current-current and current-heat current correlation function, respectively. The vertex corrections vanish and the transport integrals can be written as [23, 24, 26],

$$L_n = \frac{\sigma_0}{e^2} \int_{-\infty}^{\infty} d\omega \left(-\frac{df(\omega)}{d\omega} \right) \tau(\omega) \omega^n, \quad (4)$$

where $\tau(\omega)$ is the conduction electron scattering rate at energy ω [23, 24],

$$\frac{1}{\tau(\omega)} = cN\pi V^2 A(\omega), \quad (5)$$

with $A(\omega) = \mp \frac{1}{\pi} \text{Im} G_f(\omega \pm i0^+)$ the 4f-electron spectral function, $G_f(\omega)$ the retarded Green's function, $f(\omega) = 1/[1 + \exp(\omega/(k_B T))]$ the Fermi function, N the total number of scattering channels, σ_0 a material-specific constant, and $c = 1$ the concentration of 4f-ions. $G_f(\omega \pm i0^+)$ is obtained by the NCA, following closely Refs. [23, 24, 27].

The NCA results for CeRu₂Ge₂ are obtained for a ground state doublet and an excited quartet split by $\Delta = 0.07$ eV. It is convenient to assume an excited quartet CEF state instead of two excited doublets CEF levels. A significant change of the NCA results does not occur, since the separation between the first and the second excited state (0.021 eV) is less than their separation from the ground state (0.043 eV) [14, 15]. We used $E_f = -0.7$ eV, $E_0 = 0.7$ eV, $W = 4$ eV, and $\Gamma = 0.06$ eV to describe CeRu₂Ge₂ at ambient pressure and high temperatures ($k_B T = \Delta$), where the f-state is almost decoupled from the conduction band and the renormalisation of the bare parameters is small. The calculation yields the total number of 4f- and conduction electrons, $n_{tot} = 5.6301$, which is preserved at all subsequent calculations at different temperatures and Γ -values by adjusting μ [21].

B. Spectral functions

The spectral function $A(\omega)$ for a given value of Γ ($0.06 \text{ eV} < \Gamma < 0.2 \text{ eV}$) is calculated for a discrete set of temperatures in the range $2 \text{ K} < T < 800 \text{ K}$. The

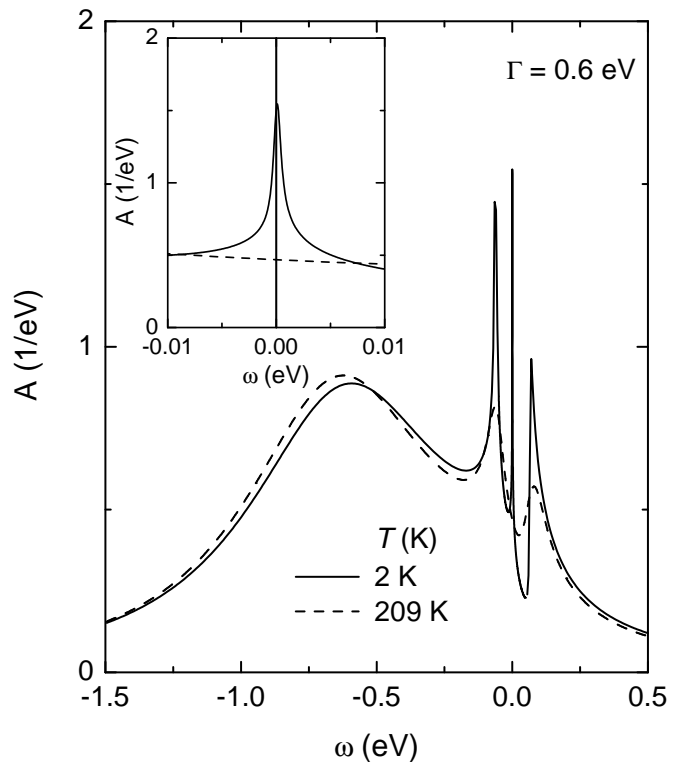


FIG. 4: Spectral function $A(\omega)$, calculated for two temperatures using $\Gamma = 0.06$ eV and $\Delta = 0.07$ eV. The broad feature just above $E_f = -0.7$ eV is the charge-excitation peak. The renormalised CEF peaks and the Kondo resonance appear close to the chemical potential μ at $\omega = 0$. The inset shows $A(\omega)$ in the vicinity of $\omega = 0$. In the low-temperature $A(\omega)$ the Kondo peak is centred at $k_B T = \omega_0 \approx 0.2$ meV.

change of the shape of $A(\omega)$ with temperature for increasing Γ -values, i.e., for enhancing the charge fluctuations, is presented in the following. Although the precise relationship between Γ and pressure is not known it seems reasonable to assume that an increase of Γ results in an increase of pressure.

Figure 4 shows $A(\omega)$ at different temperatures and for the case $\Gamma < \Delta$ and $n_f \simeq 1$. Common features to all curves are a broad charge-excitation peak somewhat above E_f (at $\omega \approx -0.59$ eV) and two features due to spin excitations of the full CEF multiplet. For $k_B T < \Delta$ these two peaks grow and sharpen. At very low temperature, an additional peak develops just above μ (inset to Fig. 4) and the low-energy part of $A(\omega)$ is characterised by three pronounced peaks [23, 24]. The two peaks centred at about $\omega_0 \pm \Delta$ are the renormalised CEF peaks, while the peak at ω_0 , which is close to μ , is the Kondo resonance. It determines the low-temperature transport properties. The energy ω_0 provides the NCA definition of the characteristic Kondo temperature, $T_0 = \omega_0/k_B$. The comparison with the numerical renormalisation group (NRG) calculations shows [28] that this T_0 is a reliable estimate of the Kondo temperature even for a doubly degenerate Anderson model. Thus, we assume that the NCA defini-

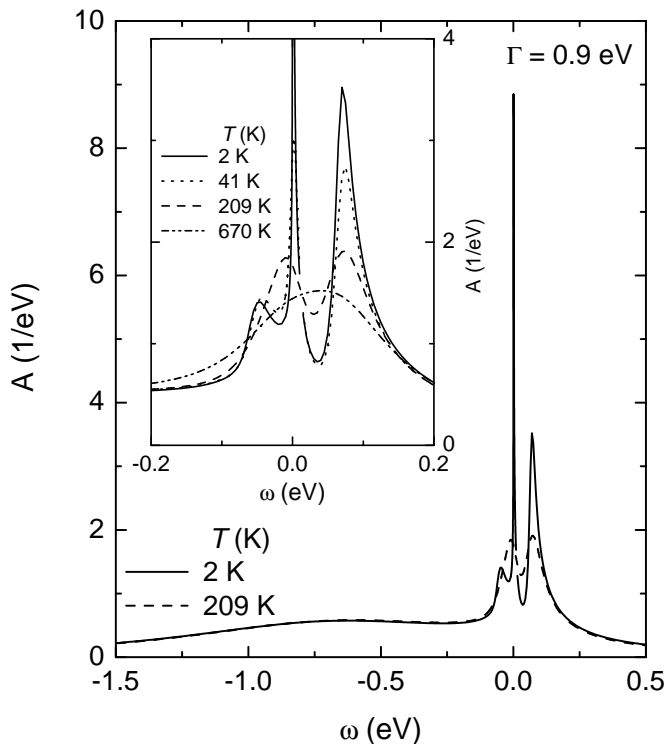


FIG. 5: Spectral function $A(\omega)$ calculated with $\Gamma = 0.09$ eV and $\Delta = 0.07$ eV for different temperatures. Here the amplitude of the charge excitation and the lower CEF peak at $\omega \approx \omega_0 - \Delta$ are strongly reduced. The two features above $\omega = 0$ are the Kondo resonance and the renormalised CEF peak at ω_0 and $\omega_0 + \Delta$, respectively. The inset shows the temperature variation of $A(\omega)$ in a smaller energy range around the chemical potential.

tion of T_0 provides the correct Kondo scale of the CEF split single-ion Anderson model as well.

For $\Gamma \geq \Delta$ (and $0.9 \leq n_f < 0.95$) the relative amplitudes of the peaks have changed (Fig. 5). At high temperatures, i.e. for $k_B T \simeq \Delta$, the only prominent feature is the low-energy resonance which is due to the exchange scattering on the full CEF multiplet ($A(\omega)$ -curve at 670 K in the inset to Fig. 5). With decreasing temperature the amplitude of the renormalised CEF peak above the chemical potential and of the Kondo resonance increase. The larger Γ with respect to Fig. 4 results in a reduced amplitude of the charge excitation peak, in a broadening of the peaks, and a shift of their positions to higher energies, whereas their separation is still Δ .

A further increase of Γ , such that $0.75 \leq n_f < 0.9$, shifts the Kondo and the CEF peak to higher energies (Fig. 6). The Kondo peak is reduced but can still be resolved as a small feature on the low-energy side of the renormalised CEF peak. A different behaviour of $A(\omega)$ is found for $\Gamma \gg 2\Delta$, i.e., $n_f < 0.8$ (inset to Fig. 6). It has only a single broad peak centred at $\tilde{E}_f \approx 0.13$ eV, the renormalised position of the virtual bound 4f-state, and $A(\omega)$ shows no splitting despite the presence of the CEF-term in the Hamiltonian. The shape of this peak

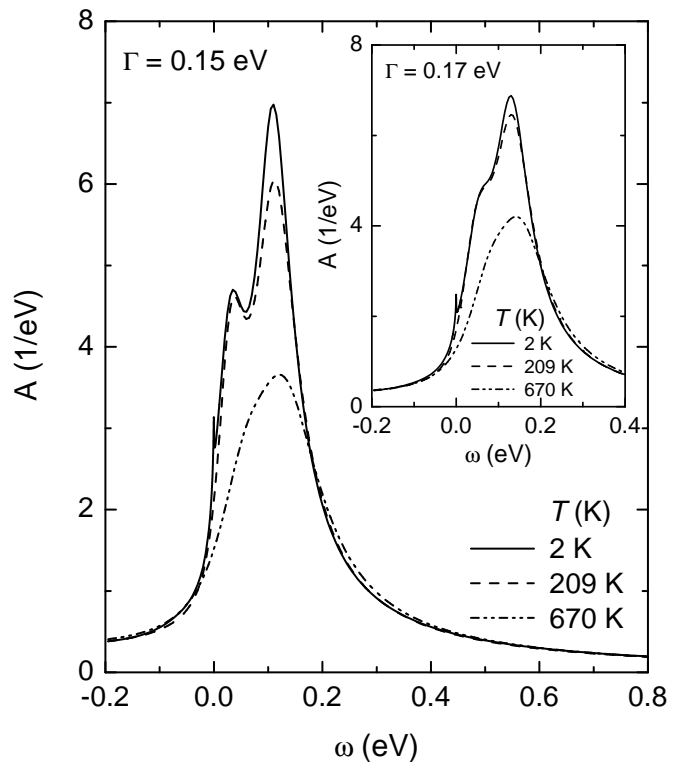


FIG. 6: Spectral function $A(\omega)$ calculated for the parameters $\Gamma = 0.15$ eV and $\Delta = 0.07$ eV at different temperatures. The Kondo resonance and the CEF peak are separated for $T \ll 670$ K. The data calculated for $T = 2$ K exhibit an artificial spike at $\omega = 0$ (see text). Inset: $A(\omega)$ calculated for $\Gamma = 0.17$ eV and $\Delta = 0.07$ eV. The Kondo peak occurs as shoulder at the low-energy side of a broad peak centred at $\tilde{E}_f \approx 0.13$ eV.

is retained at all temperatures and the Kondo resonance appears only as a weak shoulder on the low-energy side of this broad peak. Such a spectral function defines the MV regime of the Anderson model, where the relevant energy scale is $k_B T_0 = \tilde{E}_f$, which depends almost linearly on Γ [21]. The low-temperature part of $A(\omega)$ depicted in Fig. 6 clearly shows the limitations of our approach: The spike present at $\omega = 0$ is an artefact of the NCA and leads to an artificial enhancement of $\rho(T)$ and $S(T)$ at low temperatures. The consequence of these non-analytic NCA states is commented below.

C. Calculated electrical resistivity and thermopower

The moments L_n (with $n = 0, 1$) of the conduction electron scattering rate, weighted with the energy derivative of the Fermi function (eq. (4)), determine the electrical resistivity and the thermopower (eq. (2) and (3)). Thus, $\rho(T)$ and $S(T)$ reflect the form of $A(\omega)$ around the chemical potential within the Fermi window $|\omega| < 2k_B T$. The sign of $S(T)$ is positive if within the Fermi window

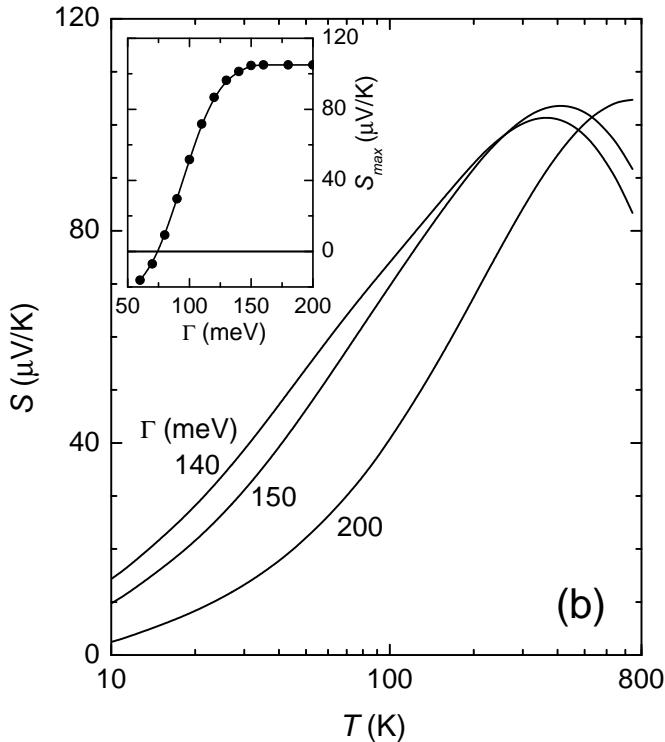
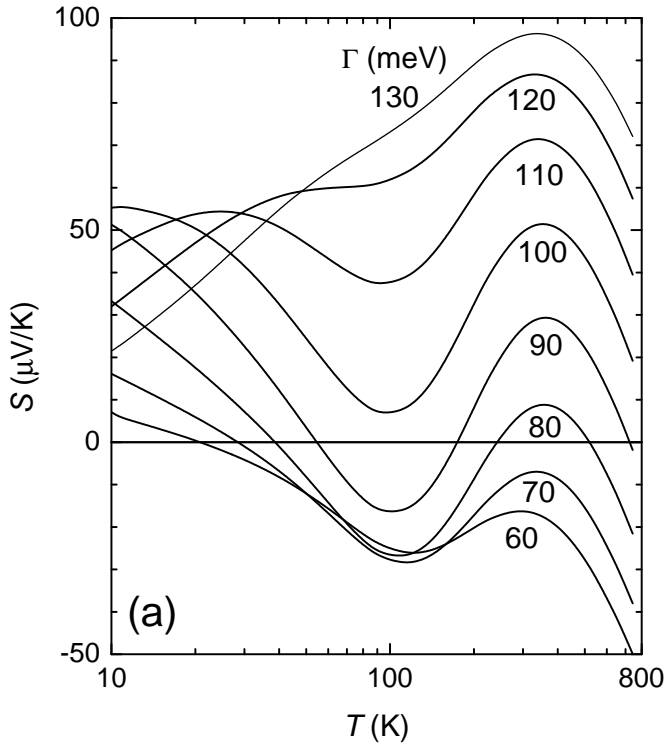


FIG. 7: (a) Temperature dependence of the calculated thermopower $S(T)$ for several small (a) and large (b) values of the hybridisation Γ and $\Delta = 0.07$ eV. The inset to (b) shows the Γ -dependence of $S_{max} \equiv S(T_S)$, the amplitude of the high-temperature maximum located at T_S in the calculated $S(T)$ -data.

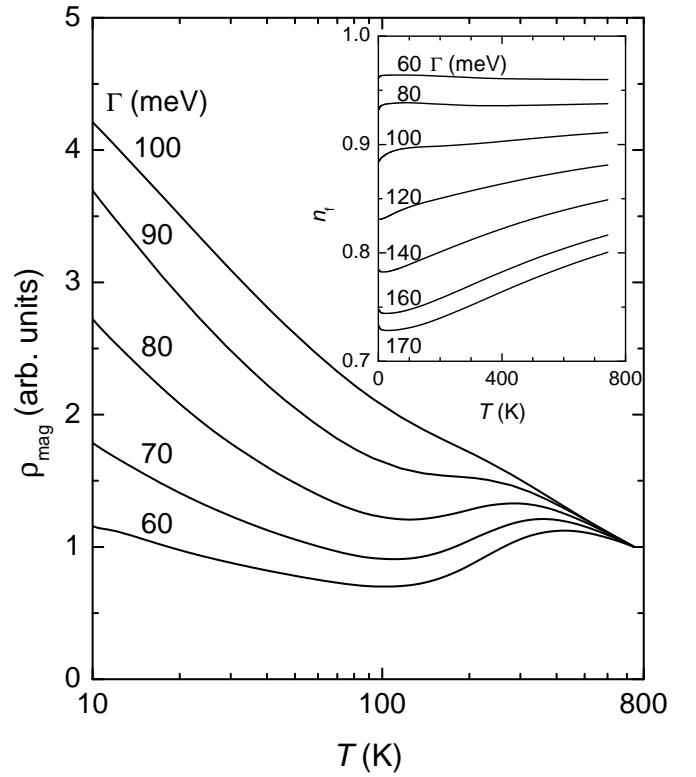


FIG. 8: Calculated temperature dependence of the electrical resistivity $\rho_{mag}(T)$ for different hybridisation Γ and $\Delta = 0.07$ eV. The enhancement of $\rho(T)$ at low temperature is an artefact of the calculation (see text). The inset shows the temperature variation of the f-electron number, n_f , at various values of Γ .

more states lie above than below the chemical potential. $S(T)$ is negative in the opposite case.

The NCA results for $S(T)$ and small Γ -values ($\Gamma \leq 100$ meV) show one well resolved maximum at $T_S \approx 300$ K and an evolution of a second maximum, T_{max}^{low} , at low temperatures (Fig. 7(a)). For $100 \text{ meV} \leq \Gamma \leq 130$ meV, the overall absolute value of $S(T)$ has increased and T_S is slightly shifted to lower temperatures. As a consequence of the appearance of the low-temperature maximum, the minimum in $S(T)$ around 100 K becomes less pronounced. T_{max}^{low} correlates with the Kondo scale T_0 . At high Γ -values, i.e., $\Gamma > 130$ meV, the shape of $S(T)$ is characterised by the high-temperature maximum which is shifted upwards in temperature (Fig. 7(b)). Its amplitude, $S_{max} \equiv S(T_S)$, increases almost linearly with Γ and saturates above $\Gamma \approx 150$ meV (inset to Fig. 7(b)).

Figure 8 depicts the calculated $\rho_{mag}(T)$ for several (small) values of Γ . The low-temperature $\rho_{mag}(T)$ exceeds that at high temperature, since the NCA overestimates $A(\omega)$ at small ω . Nevertheless, the logarithmic increase, as temperature decreases towards T_0 , is preceded by the formation of a high-temperature maximum well above T_0 . Its position correlates very well with the maximum at T_S in $S(T)$. The maximum in $\rho_{mag}(T)$ becomes less pronounced and is masked for $\Gamma > 100$ meV due to

the artificially large $A(\omega)$ around μ . The occurrence of these non-analytic NCA states in $A(\omega)$ for large Γ -values has a minor effect on the 4f-electron number, n_f (inset to Fig. 8). n_f is the integral of $A(\omega)$ multiplied by the Fermi function. In the MV regime ($\Gamma > 2\Delta$) $n_f(T)$ decreases strongly from the high-temperature limit to $n_f \approx 0.7$ at low temperatures. The small increase at the lowest temperature results from the spike in $A(\omega)$. In the Kondo regime ($\Gamma < \Delta$) $n_f \approx 1$ is almost temperature independent. The variation of $n_f(T)$ with Γ reflects the change of regimes.

The strong increase of $\rho_{mag}(T)$ and the enhanced $S(T)$ at low temperature (for $T \ll T_0$) is a consequence of the spike in $A(\omega)$. This becomes particularly severe for large Γ values ($\Gamma > 100$ meV). In this region the characteristic temperature scale T_0 increases very rapidly with Γ and $A(\omega)$ acquires non-analytic NCA states already at rather high temperatures (inset to Fig. 6). The integral L_0 is strongly underestimated, resulting in a $\rho_{mag}(T)$ which is too large (eq. (2)). The integral L_1 is less affected, because the artificial NCA states are removed by the additional ω -factor in eq. (4). Thus, the shape of $S(T) \simeq L_1^{NCA}/L_0^{NCA}$ seems to be qualitatively correct, even for large Γ -values, but the magnitude of the low-temperature $S(T)$ is enhanced, since $1/L_0^{NCA} \gg 1/L_0^{exact}$. These difficulties are well known [23, 24] and can be solved easily in the Kondo limit, where the model has a unique Kondo scale, T_0 . The latter can be calculated in the LM regime, where the NCA is reliable. Once T_0 is known, the low-temperature transport properties can be inferred from the universal power laws $\rho(T) \propto 1 - a(T/T_0)^2$ and $S(T) \propto b(T/T_0)$ (where a and b follow from the Sommerfeld expansion) which hold in the FL regime. Thus, combining the NCA and the FL theory, we can discuss the experimental data at all temperatures at which the single-ion approximation holds.

IV. DISCUSSION

The evolution of the calculated transport coefficients described above has several features of the pressure-induced changes in $\rho_{mag}(T)$ and $S(T)$ of CeRu₂Ge₂ presented in Sec. II. In the following, the evolution of the transport properties is related to the modifications of $A(\omega)$ caused by the increase of Γ and compared to the experimental data. However, the above mentioned limitations of the theoretical approach should be kept in mind.

As far as the NCA results of $\rho_{mag}(T)$ are concerned, the comparison of the theoretical and experimental data is limited to temperatures above about 100 K. This is due to the fact that the NCA yields an enhanced $A(\omega)$ at small ω and large Γ and the calculated $\rho_{mag}(T)$ increase strongly towards low temperatures. In addition, the single-site model leads to a low-temperature saturation of $\rho_{mag}(T)$, which is not observed in stoichiometric compounds. Thus, the NCA results for $\rho_{mag}(T)$ can only

be used for a qualitative discussion of the experimental data at low pressure. The clear high-temperature maximum and the subsequent shallow minimum, present in $\rho_{mag}(T)$ for small hybridisation, are seen in the experimental behaviour of $\rho_{mag}(T)$ for $p \leq 3.4$ GPa (Fig. 1). Furthermore, the weak Γ -dependence of the maximum position in the calculated $\rho_{mag}(T)$ is also observed in the experimental data.

The clear features in the calculated $S(T)$ -data and their evolution with Γ make a detailed comparison with the effect of pressure on $S(T)$ possible. The ambient pressure $S(T)$ is negative for temperatures below 300 K (Fig. 2). This shape of $S(T)$ corresponds to that calculated for $\Gamma = 60$ meV (Fig. 7(a)). It results from the fact, that within the Fermi window less spectral weight is present above than below μ . The difference, however, is small, which explains the small negative value of $S(T)$. For $k_B T < \Delta$ the amplitude of the renormalised CEF peak in $A(\omega)$ below the chemical potential increases (Fig. 4) and $S(T)$ attains slightly larger negative values in agreement with the ambient pressure data. At even lower temperature, the development of the Kondo resonance leads to more spectral weight above than below μ and $S(T)$ starts to increase. This leads to the evolution of the minimum around 100 K and $S(T) > 0$ below 20 K. The minimum is clearly present in the experimental data, whereas the occurrence of the long-range magnetic order and the opening of a spin-gap [29] conceals the positive maximum at low temperature. The features in the experimental $S(T)$ data below 10 K are related to magnetic order and cannot be accounted for in the theory, since the single-ion approximation is not suited for the ordered phase of stoichiometric compounds. Here the 4f-electrons become coherent at low enough temperatures, leading to magnetic transitions or to the formation of a heavy FL, like in CeRu₂Ge₂ at low or high pressure, respectively.

For $\Gamma > \Delta$, more spectral weight is present above than below μ . In this case the exchange scattering on the full CEF multiplet yields $S(T) > 0$ as experimentally observed for $p \geq 5.7$ GPa below 300 K. Reducing the temperature shifts spectral weight below the chemical potential (Fig. 5) and $S(T)$ decreases. This redistribution leads again to a small positive low-temperature maximum at $T = T_{max}^{low} \simeq T_K^H$. The minimum in the $S(T)$ -curves can be slightly negative or positive, depending on the value of Γ with respect to Δ . This becomes evident for $\Gamma = 90$ meV and 100 meV (Fig. 7(a)) and in the experimental data for $p = 3.4$ GPa and $p = 5.7$ GPa (Fig. 2). $S(T)$ exhibits only a shallow minimum or a shoulder below T_S , like the curve for $\Gamma = 120$ meV in Fig. 7(a). The equivalent experimental data are those measured at 7.0 GPa depicted in Fig. 2.

The Kondo resonance appears only as a shoulder at the broad high-temperature maximum in the calculated $S(T)$ -curves for $\Gamma > 2\Delta$. In this region a drastic change of the relative spectral weight of the peaks in $A(\omega)$ occurred and the Kondo resonance represents only a negli-

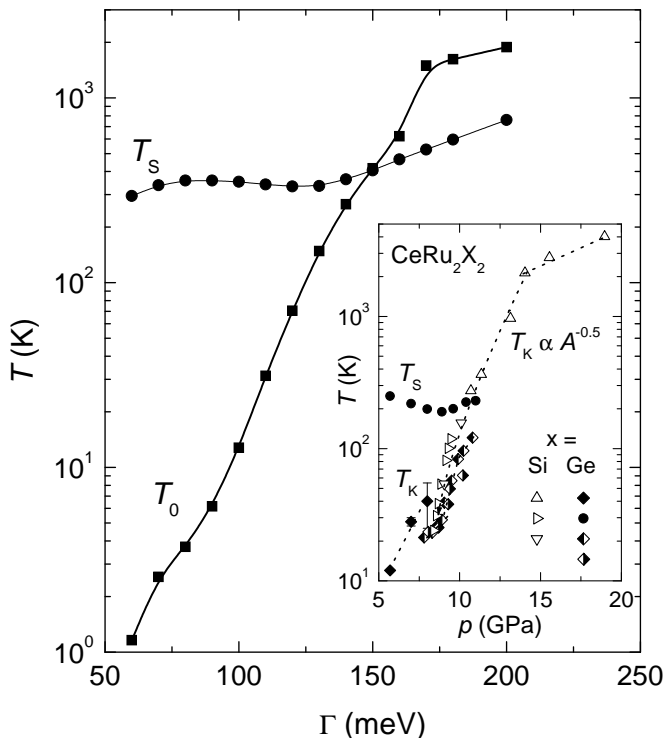


FIG. 9: T_S , the position of the high-temperature maximum in the calculated $S(T)$, and T_0 , the characteristic temperature scale, vs. hybridisation Γ . T_0 corresponds to T_K (small Γ), T_K^H (intermediate Γ), and \tilde{E}_f (large Γ). The inset shows the experimental data of T_S and T_K of CeRu_2Ge_2 and $T_K \propto \sqrt{A}$ of CeRu_2Si_2 take from literature [30, 31, 32]. The latter are shifted in pressure by 8.4 GPa (see text).

gible correction to the spectral weight within the Fermi window. $S(T)$ is always positive and grows monotonically towards the high-temperature maximum at $T_0 \propto \tilde{E}_f$ (Fig. 7(b)) as experimentally observed for $p > 10$ GPa (inset to Fig. 2). It is noteworthy, that the almost linear increase of the calculated value of $S(T_S)$ is in qualitative agreement with the experimental findings (inset to Fig. 7(b)) [10].

Figure 9 shows the Γ -dependence of T_0 and T_S determined from $A(\omega)$ and the calculated $S(T)$ -curves, respectively. The NCA values of T_0 obtained for $\Gamma \ll \Delta$ are very well approximated by the scaling expression $T_0 = T_K(g)$ [23, 24]. For a ground state doublet and an excited quartet it is $T_K(g) \simeq Wg^{1/2} \exp\{-1/(2g)\}(W/\Delta)^{4/2}$. The exponent 4/2 reflects the assumption of an excited quartet instead of a doublet state. The Kondo resonance is due to spin excitations of the CEF doublet, whereas the Kondo temperature is enhanced by $(W/\Delta)^2$ due to the presence of excited CEF states. For intermediate values of Γ (e.g. $\Gamma \approx 100$ meV), the relationship between T_0 and the coupling constant is $T_0 = T_K^H \simeq Wg^{1/2} \exp\{-1/(2g)\}[W/(\Delta + T_K)]^{4/2}$.

The T_0 -line in the (T, Γ) -phase diagram (Fig. 9) separates the FL region from the LM region and the MV

regime. In the Kondo regime, an increase of temperature at constant hybridisation gives rise to a transition from the FL regime to the LM regime of a CEF ground state, and then to the LM regime of a full CEF multiplet. The crossover between the two LM regimes is accompanied by the minimum of $S(T)$ (Fig. 2 and 7). At low coupling ($\Gamma \leq 90$ meV and $T_0 \simeq T_K$), the thermopower becomes negative at the crossover from the FL to the LM regime and it stays negative in the LM regime of a full CEF multiplet. At intermediate coupling ($\Gamma \approx 100$ meV and $T_0 \simeq T_K^H$), the FL and the LM regimes are too close for the sign-change to occur, and the crossover is indicated by a shallow minimum between two asymmetric peaks or just a shoulder in $S(T)$. For larger Γ -values, the crossover is from the FL to a MV regime but the FL scale is large, $T_0 \propto g$, and $S(T)$ grows monotonically towards the high-temperature maximum. The variation of the hybridisation at constant temperature changes the shape of the spectral function from a typical LM to a typical FL shape.

The phase diagram deduced from the single-impurity Anderson model calculations is in rather good agreement with the experimental one. In the inset to Fig. 9 the pressure dependence of the experimentally obtained T_K -values of CeRu_2Ge_2 (already shown in Fig. 3) are replotted together with the data of CeRu_2Si_2 . The $T_K(p)$ -data of CeRu_2Si_2 were calculated from the measured $A(p)$ -dependence [30, 31, 32] using the scaling relation $T_K \propto \sqrt{A}$ with the assumption $T_K = 24$ K at ambient pressure [19]. In order to compare the CeRu_2Si_2 data with those of CeRu_2Ge_2 , the former had to be shifted by 8.4 GPa [10]. On the verge of the magnetic instability ($p \simeq 7.8$ GPa) but still in the magnetic phase, the $T_K(p)$ -variation detected with the $S(T)$ experiment, seems to confirm the exponential increase of T_0 with Γ . The change of the $T_0(\Gamma)$ -dependence at larger Γ is also seen in the experimental data above the magnetic instability, where the FL regime is entered. Here, the $T_K(p) \propto \sqrt{A(p)}$ variation for CeRu_2Ge_2 as well as CeRu_2Si_2 is different to the $T_K(p)$ dependence deduced from the $S(T)$ -data of CeRu_2Ge_2 (Fig. 3 and inset to Fig. 9). The crossover into the MV regime, where $T_0 \propto \tilde{E}_f$, yields to a reduced pressure dependence (data only for CeRu_2Si_2) in agreement with the calculated $T_0(\Gamma)$ -dependence for $\Gamma > 170$ meV. It is interesting to note that the characteristic energy scales of a local and a coherent FL do not seem to differ very much, so that the universal power laws of a coherent FL provide an estimate of the single-impurity scale T_0 . However, a proper treatment of the low-temperature and high-pressure properties requires a lattice model.

The NCA used to describe the pressure-induced features in CeRu_2Ge_2 is not restricted to this compound. Other ternary Ce-compounds like CeCu_2Si_2 or CePd_2Si_2 can also be described, if the parameters are adjusted appropriately. The method works also for Yb-compounds if the decrease of the coupling between the 4f-states and the conduction band with pressure is taken into account.

V. CONCLUSIONS

A qualitative understanding of the pressure-induced changes in the electrical resistivity $\rho(T)$ and thermopower $S(T)$ of CeRu₂Ge₂ was developed in the framework of the single-site Anderson model. The evolution of $\rho(T)$ and $S(T)$ with pressure was accounted for by the increase of the 4f-conduction band electron hybridisation Γ . The calculated spectral functions $A(\omega)$ show that the temperature-induced redistribution of spectral weight yields several of the pronounced features observed in the measured transport quantities. The position of the peak in $A(\omega)$ close to the chemical potential gives a very reliable estimate of the characteristic Kondo temperature T_0 at low temperature. The crossovers between various fixed points of the Anderson model and the redis-

tribution of the single-particle spectral weight within the Fermi window explain the hybridisation dependence of the transport coefficients and the seemingly complicated temperature and pressure dependences of experimental $S(T)$ -data. The Γ -dependence of the characteristic temperature scale T_0 is in qualitative agreement with the experimentally determined $T_K(p)$ -variation.

Acknowledgments

We thank T. C. Kobayashi and M. Malquarti for assistance during the thermopower measurements. H. W. is grateful to B. Schmidt for many stimulating discussions. The work was partly supported by the Swiss National Science Foundation.

-
- [1] D. Jaccard, K. Behnia, and J. Sierro, *Phys. Lett. A* **163**, 475 (1992).
 - [2] E. M. Levin, R. V. Lutsiv, L. D. Finkel'shtein, N. D. Samsonova, and R. I. Yasnitskii, *Sov. Phys. Solid State* **23**, 1403 (1981).
 - [3] D. Jaccard and J. Sierro, in *Valence Instabilities*, edited by P. Wachter and H. Boppert, North-Holland, Amsterdam, p. 409 (1982).
 - [4] D. Jaccard, J. M. Mignot, B. Bellarbi, A. Benoit, H. F. Braun, and J. Sierro, *J. Magn. Magn. Mater.* **47&48**, 23 (1985).
 - [5] A. Amato, D. Jaccard, J. Sierro, P. Haen, P. Lejay, and J. Flouquet, *J. Low Temp. Phys.* **77**, 195 (1989).
 - [6] A. Amato, D. Jaccard, J. Flouquet, F. Lapiere, J. L. Tholence, R. A. Fisher, S. E. Lacy, J. A. Olsen, and N. E. Phillips, *J. Low Temp. Phys.* **68**, 371 (1987).
 - [7] P. Link, D. Jaccard, and P. Lejay, *Physica B* **225**, 207 (1996).
 - [8] P. Link, D. Jaccard, and P. Lejay, *Physica B* **223&224**, 303 (1996).
 - [9] C. Fierz, D. Jaccard, J. Sierro, and J. Flouquet, *J. Appl. Phys.* **63**, 3899 (1988).
 - [10] H. Wilhelm and D. Jaccard, *Phys. Rev. B* **69**, 214408 (2004); cond-mat/0402187.
 - [11] A. K. Bhattacharjee and B. Coqblin, *Phys. Rev. B* **13**, 3441 (1976).
 - [12] V. Zlatic, B. Horvatic, I. Milat, B. Coqblin, G. Czucholl, and C. Grenzebach, *Phys. Rev. B* **68**, 104432 (2003).
 - [13] D. Jaccard, E. Vargoz, K. Alami-Yadri, and H. Wilhelm, *Rev. High Pressure Sci. Technol.* **7**, 412 (1998); cond-mat/9711089.
 - [14] R. Felten, G. Weber, and H. Rietschel, *J. Magn. Magn. Mater.* **63&64**, 383 (1987).
 - [15] A. Loidl, K. Knorr, G. Knopp, A. Krimmel, R. Caspary, A. Bohm, G. Sparr, C. Geibel, F. Steglich, and A. P. Murani, *Phys. Rev. B* **46**, 9341 (1992).
 - [16] H. Wilhelm, K. Alami-Yadri, B. Revaz, and D. Jaccard, *Phys. Rev. B* **59**, 3651 (1999).
 - [17] H. Wilhelm and D. Jaccard, *Solid State Commun.* **106**, 239 (1998).
 - [18] F. Bouquet, Y. Wang, H. Wilhelm, D. Jaccard, and A. Junod, *Solid State Commun.* **113**, 367 (2000).
 - [19] M. J. Besnus, J. P. Kappler, P. Lehmann, and A. Meyer, *Solid State Commun.* **55**, 779 (1985).
 - [20] P. Haen, H. Bioud, and T. Fukuhara, *Physica B* **281&282**, 59 (2000).
 - [21] V. Zlatic and R. Monnier, *to be published*.
 - [22] A. C. Hewson, *The Kondo Problem to Heavy Fermions*, Cambridge University Press, Cambridge (1993).
 - [23] N. E. Bickers, D. L. Cox, and J.W. Wilkins, *Phys. Rev. B* **36**, 2036 (1987).
 - [24] N. E. Bickers, *Rev. Mod. Phys.* **59**, 845 (1987).
 - [25] G. D. Mahan, *Many-Particle Physics* (Plenum, New York, 1981).
 - [26] G. D. Mahan, in *Solid State Physics*, Academic Press, San Diego, Vol. 51, p. 81 (1998).
 - [27] R. Monnier, L. Degiorgi, and B. Delley, *Phys. Rev. B* **41**, 573 (1990).
 - [28] T. A. Costi, J. Kroha, and P. Wolfle, *Phys. Rev. B* **53**, 1850 (1996).
 - [29] S. Raymond, P. Haen, R. Calemczuk, S. Kambe, B. Fak, P. Lejay, T. Fukuhara, and J. Flouquet, *J. Phys. Condens. Matter* **11**, 5547 (1999).
 - [30] K. Payer, P. Haen, J.-M. Laurant, J.-M. Mignot, and J. Flouquet, *Physica B* **186-188**, 503 (1993).
 - [31] J.-M. Mignot, A. Ponchet, P. Haen, F. Lapiere, and J. Flouquet, *Phys. Rev. B* **40**, 10917 (1989).
 - [32] J. D. Thompson, J. O. Willis, C. Godart, D. E. MacLaughlin, and L. C. Gupta, *J. Magn. Magn. Mater.* **47&48**, 281 (1985).